H∞ Control of WRIM Driven Flywheel Storage System to Ride-Through Grid Voltage Dips

Ahmed LAZRAK, Ahmed ABBOU

Department of Electrical Engineering, Mohammadia School of Engineering,
Mohammed V University in Rabat, Avenue Ibn Sina 765, 10090 Rabat, Morocco

lazrak.ahmedd@gmail.com, abbou@emi.ac.ma

DOI: 10.15598/aeee.v18i1.3546

Abstract. *Flywheel Energy Storage Systems (FESSs) are commonly integrated with wind farms to help them to provide many grid services, including frequency control, voltage control, and power smoothing. Although such systems are not concerned by the severe grid code requirements, their ability to ride-through voltage dips is important to ensure better stability of the power grid. In this paper, the authors propose a robust H∞ current controller for a Wound Rotor Induction Machine (WRIM) based FESS during grid voltage dips. The proposed H∞ controller decreases the negative effects of voltage dips in the WRIM system, such as the rotor over-currents and the active power oscillations. On the other hand, it also guarantees the robustness in the presence of parameter perturbation. The proposed controller is designed using a modified mixed-sensitivity H∞ technique to take into consideration grid disturbances and parameter perturbation. Finally, simulations are made in MATLAB/Simulink using SimPowerSystems to verify the effectiveness of the H∞ controller under grid voltage dips with WRIM parameter perturbation. The simulation results show that the proposed H∞ controller can improve the stability of the WRIM based FESS subject to grid voltage dips and guarantee the robustness with parameter perturbation.*

Keywords

FESS, H∞ controller, voltage dips, wind farm, WRIM.

1. Introduction

With regard to the progressive exhaustion of fossil energy, new alternative energies are considered key tools for reducing carbon dioxide emissions. Among these renewable energies, wind is the fast-growing source of electricity in the world. In 2018, nearly 51.3 GW of new capacity were installed worldwide, bringing the global total to around 591 GW [1].

Nevertheless, with rising penetration of wind energy and their variable nature, grid instability is a major concern. As these wind energy sources may lead to frequency and voltage instability, especially for a weak part of the grid [2]. In addition, the disconnection of wind generators from the power grid during grid faults may amplify grid instability issues [3].

In recent years, Flywheel Energy Storage System (FESS) has gained increasing attention because it can support wind energy sources to provide many grid services, including frequency control and power smoothing [4], and [5]. Considering their technical characteristics, fast response is the key to the FESS for providing the above-mentioned services and also for improving the ride-through capability of wind farms [6].

Among the existing electrical machines used in FESSs, Permanent Magnet Synchronous Machines (PMSM) and Induction Machines (IM) are perhaps the most commonly employed machines [7], [8], [9], and [10]. The Wound-Rotor Induction Machine (WRIM) is also of particular interest in the field of FESS, where it has the advantages of smaller rating converters, and decoupled control of active and reactive power [11], and [12]. Various advanced control strategies have been developed to control the FSS based WRIM for wind power smoothing such as; Fuzzy logic combined with sliding mode control [13], artificial neural network [14], adaptive neuro-fuzzy control [15], and adaptive wavelet fuzzy neural network combined with nonlinear predictive control [6].

Flywheel Energy Storage Systems (FESSs) are very susceptible to grid voltage dips. This is particularly true for FESSs based WRIMs that employ reduced converters in their design. Faults in the power system, even far away from the FESS, could cause grid voltage dips. This will result in an overcurrent on the rotor circuit of the WRIM and consequently may lead to a protective disconnection of the FESS from the power grid.

Due to their simple structure, PI controllers are the most common controllers used for WRIM control [11], and [16]. However, they have operating characteristics that result in excessive rotor currents during voltage dips, and its performance is not guaranteed under parameter perturbation [17]. This is due to the fact that PI controllers have limited bandwidth and gain margin. Therefore, different advanced control strategies such as neuro-fuzzy control [18], neural sliding mode control [19], input-output feedback linearization [20], and sliding mode combined with direct power control [21], have been used to enhance the fault ride-through ability of grid-connected WRIMs. Other methods based hardware implementation has also been proposed in the literature [22].

H∞ control has found numerous applications in electrical field control, such as wind power [23], Uninterruptible Power Supplies (UPS) [24], Dynamic Voltage Restorer (DVR) [25], and Power System Stabilizer (PSS) [26], etc. The mixed-sensitivity H∞ control is seen to be a powerful tool for robust controller design achieving Robust Stability (RS) and Robust Performance (RP) under system uncertainty [23]. In this approach, weights functions are used to shape the magnitudes of closed-loop transfer functions, such as sensitivity function S and the complementary sensitivity function T. An alternative to mixed-sensitivity H∞ control is the H∞ loop shaping synthesis [27]. This method combines the H∞ robust stabilization using normalized coprime factorization with the classical loop shaping. Such designs are formulated as an H∞ optimal control problem [28].

Considering the benefits of FESSs for wind turbines, their stability and robustness during grid voltages dips are very important. Although FESSs are not concerned by the severe grid code requirements, they must stay connected to the grid during voltage dips to ensure better stability of the electric grid. In this context, this work proposes a robust H∞ controller design of WRIM that can guarantee uninterrupted operation of the flywheel storage system during and after grid voltage dips. The main contribution of this paper is the design of a robust H∞ current controller which will decrease the negative effects of voltage dips in the WRIM system, such as rotor over-currents and active power oscillations, and guarantee the system RS and RP during grid voltage dips with parameter perturbation.

This work is organized as follows. First, the influence of grid voltage dip and WRIM parameter perturbation on the rotor currents is analyzed in Sec. 2. Next, the H∞ current controller is designed, and the weights functions are selected to guarantee the system RS and RP in Sec. 3. Finally, simulations in Matlab/Simulink are presented in Sec. 4. to evaluate the performance of the proposed H∞ controller during grid voltage dips with parameter perturbation, followed by a conclusion in Sec. 4.

2. System Modelling

2.1. System Overview

A flywheel energy storage system incorporating a WRIM is connected to the point of common coupling of a wind farm with the power grid, as shown in Fig. 1. Adjusting the rotor speed of the WRIM makes the flywheel either release or absorb energy in order to smooth the wind power delivered into the grid.

2.2. Wind Farm Modelling

In this work, six wind turbines based on doubly fed induction generators that operate identically constitute a wind farm of 9 MW. Each wind turbine presents a rated power of 1.5 MW.

Due to various losses in a wind turbine, the power extracted from the wind is given by [29]:

$$P = \frac{1}{2} C_P(\beta, \lambda) \rho S v_w^3, \tag{1}$$

where: S is the surface swept by the blades of the turbine in (m^2), ρ is the density of the air in (kg·m^{-3}), v_w is the wind speed in (m·s^{-1}), C_P is the power coefficient (-), λ is the tip speed ratio, and β is the blade pitch angle in (°).

The tip speed ratio λ is defined by the following equation:

$$\lambda = \frac{R\Omega_t}{v_w}. \tag{2}$$

The expression of C_P is approached for a 1.5 MW turbine using the following nonlinear function [30]:

$$\frac{1}{\lambda_i} = \frac{1}{\lambda + 0.08\beta} - \frac{0.035}{\beta^3 + 1}, \tag{3}$$

$$C_P(\alpha, \beta) = C_1 \left(\frac{C_2}{\lambda_i} - C_3\beta - C_4 \right) e^{\left(-\frac{C_5}{\lambda_i}\right)}. \tag{4}$$

The values of coefficients C_1 to C_5 are given in Tab. 1.

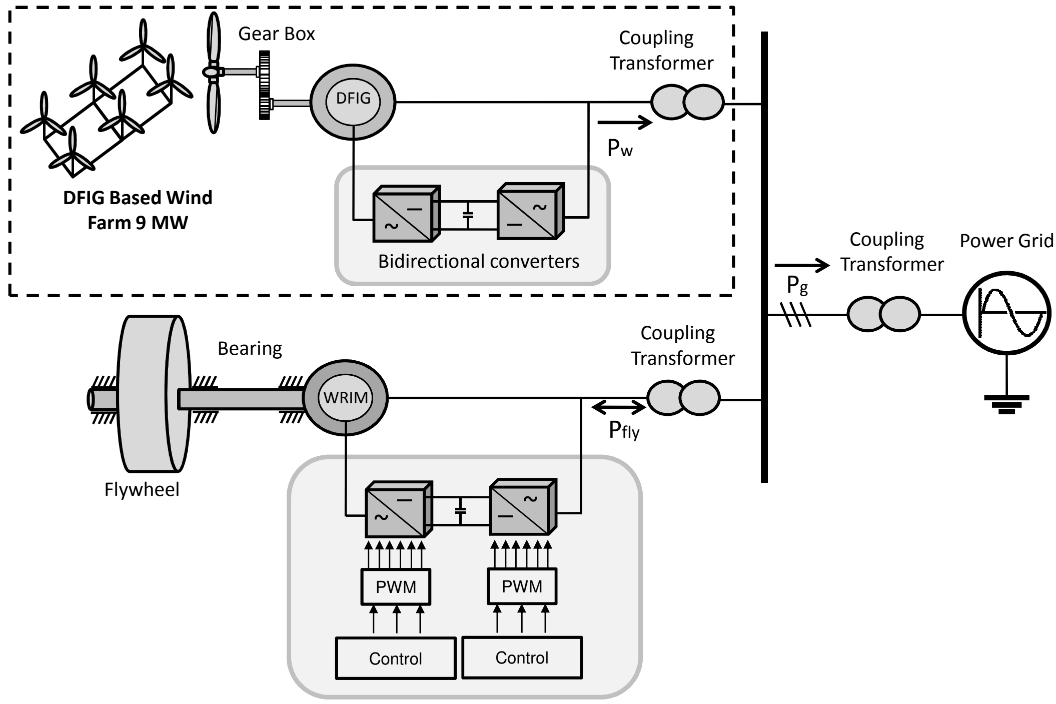

Fig. 1: WRIM driven flywheel energy storage system for wind power smoothing.

Figure 2 demonstrates the efficiency coefficient curve C_P against the tip speed ratio λ and the blade pitch angle β. We obtain a maximum value of C_P equal to 0.4382 for a blade pitch angle $\beta = 0$ ° and for an optimum value of the speed ratio ($\lambda_{opt} = 6.32$). Maximum Power Point Tracking (MPPT) is used to capture the maximum power from each wind turbine and therefore increase the overall performance of the wind farm. Therefore, the pitch angle is kept at the optimal value $\beta = 0$ °.

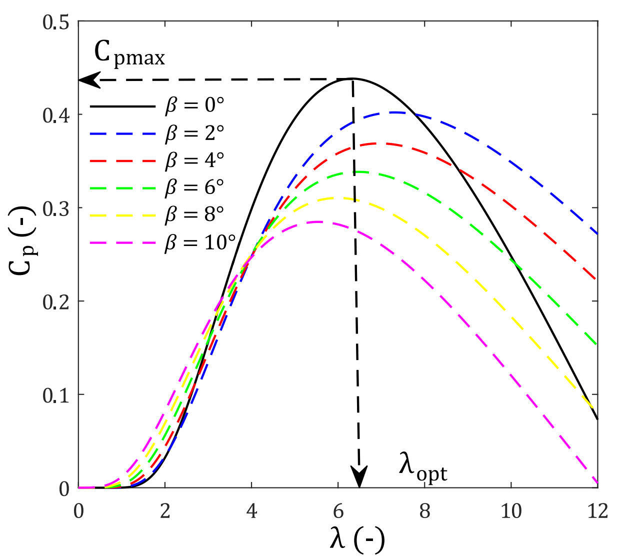

Fig. 2: Efficiency coefficient characteristic for the wind turbine.

Tab. 1: The values of coefficients C_1 to C_5.

C_1	C_2	C_3	C_4	C_5
0.73	151	0.58	13.2	18.4

2.3. WRIM Driven FESS Modelling

The flywheel energy storage system is modeled as a WRIM coupled with a rotating mass that stores the electrical power as kinetic energy. The kinetic energy stored in the flywheel energy storage system is proportional to its inertia J_f and the rotational speed of the WRIM w_{rf} as shown in Eq. (5):

$$E_{fly} = \frac{1}{2} J_f w_{rf}^2, \tag{5}$$

In order to smooth the wind power injected into the grid, the kinetic energy of the FESS is determined by [13]:

$$E_{fly} = \int P_f \mathrm{d}t = \int (P_g - P_{wf})\, \mathrm{d}t, \tag{6}$$

where, P_f is the reference active power exchanged between the FESS and the grid, P_{wf} is the filtered wind power, and P_g is the desired grid power.

When the reference active power P_f is negative, it indicates that the WRIM driven FESS injects the power into the grid. While positive power indicates that the FESS stores the wind power.

Since the WRIM can be regarded as traditional IM with non-zero rotor voltages, its dynamic model in the dq-synchronous reference frame can be expressed as in Eq. (7), Eq. (8) and Eq. (9) [31]:

$$\begin{cases} v_{dsf} = R_s i_{dsf} + \frac{\mathrm{d}\varphi_{dsf}}{\mathrm{dt}} - w_{sf}\varphi_{qsf}, \\ v_{qsf} = R_s i_{qsf} + \frac{\mathrm{d}\varphi_{qsf}}{\mathrm{dt}} + w_{sf}\varphi_{dsf}, \end{cases} \tag{7}$$

$$\begin{cases} v_{drf} = R_r i_{drf} + \frac{\mathrm{d}\varphi_{drf}}{\mathrm{dt}} - (w_{sf} - w_{rf})\,\varphi_{qrf}, \\ v_{qrf} = R_s i_{qrf} + \frac{\mathrm{d}\varphi_{qrf}}{\mathrm{dt}} + (w_{sf} - w_{rf})\,\varphi_{drf}, \end{cases} \tag{8}$$

$$\begin{cases} \varphi_{dsf} = L_s i_{dsf} + L_m i_{drf}, \\ \varphi_{qsf} = L_s i_{qsf} + L_m i_{qrf}, \\ \varphi_{drf} = L_r i_{drf} + L_m i_{dsf}, \\ \varphi_{qrf} = L_r i_{qrf} + L_m i_{qsf}, \end{cases} \tag{9}$$

where the subscripts "s" and "r" represent the stator and rotor R_s and R_r are resistances of the stator and rotor, $L_{\sigma s}$ and $L_{\sigma r}$ are the stator and rotor leakage inductances, L_m is the magnetizing inductance, $L_s = L_{ls} + L_m$ and $L_r = L_{lr} + L_m$ are the stator and rotor winding total self-inductances, φ_{sf} and φ_{rf} are the stator and rotor magnetic flux linkages, v_{sf} and v_{rf} are the stator and rotor voltages, i_{sf} and i_{rf} are the stator and rotor currents, w_{sf} is the electrical angular speed, and w_{rf} is the rotor angular speed.

3. Uncertain Model of WRIM Driven FESS

Since our main objective in this work is protecting the converters and the machine under grid voltage dips against rotor over-current, the FESS model will focus on the rotor current loop control. In this work, the system uncertainty is described as WRIM parameter perturbation and grid voltage dips. Based on Eq. (7) and Eq. (8), an uncertain WRIM model can be described as:

$$\begin{cases} \dot{x} = (\mathbf{A} + \delta_A)x + (\mathbf{B} + \delta_B)u + (\mathbf{B_d} + \delta_{B_d})(1 + \delta_d)d, \\ y = \mathbf{C}x, \end{cases} \tag{10}$$

where, $\vec{x} = \begin{bmatrix} i_{dsf} & i_{qsf} & i_{drf} & i_{qrf} \end{bmatrix}$ is the state variable vector, $\vec{u} = \begin{bmatrix} u_{drf} & u_{qrf} \end{bmatrix}$ is the input vector, $\vec{d} = \begin{bmatrix} u_{dsf} & u_{qsf} \end{bmatrix}$ is the disturbance input vector, and $\vec{y} = \begin{bmatrix} i_{drf} & i_{qrf} \end{bmatrix}$ is the output vector.

The matrices $\mathbf{A}$, $\mathbf{B}$, $\mathbf{B_d}$, and $\mathbf{C}$ are given by Eq. (11), Eq. (12), Eq. (13), and Eq. (14), respectively, where δ_A, δ_B and $\delta_{\mathbf{B_d}}$ present the uncertain part of the matrices $\mathbf{A}, \mathbf{B}$, and $\mathbf{C}$, respectively. Here, ± 50 % perturbation with respect to the nominal values of the parameters R_r, L_m, $L_{\sigma s}$ and $L_{\sigma r}$ has been considered. The grid voltage dip is presented in the frequency domain using a multiplicative factor δ_d, satisfying $\| (1 + \delta_d)d(w) \|_\infty \leq 1$.

Figure 4 illustrates the frequency characteristics of the uncertain model based on Eq. (10). The bode plots from u_{dsf} to i_{drf} and from u_{drf} to i_{def} are shown in Fig. 4(a) and Fig. 4(b), respectively. The curve marked with '+' represents the nominal model, while the uncertain models are shown by the other curves. It can be seen that the grid voltage disturbance and the WRIM parameter perturbation have an influence on the rotor current control.

4. H∞ Current Controller Design

4.1. H∞ Controller Structure Design

Figure 3 shows the control structure for the rotor side converter of the WRIM. The proposed control ensures the wind power smoothing by adjusting the WRIM speed when a voltage dip occurs. K∞ is the rotor current controller which is designed based on mixed-sensitivity H∞ control. The standard S/KS mixed sensitivity design with an additional weight W_0 to describe the multiplicative output uncertainty is adopted in this work, as shown in Fig. 5.

The grid voltage is considered as an external disturbance, and therefore, $G_d(s) = \mathbf{C}(sI - \mathbf{A})^{-1}\mathbf{B_d}$ is also added as an input to the S/KS mixed sensitivity design. The parameter uncertainties are represented by unstructured multiplicative output uncertainty Δ which satisfies $\| \Delta \|_\infty \leq 1$, such as $G_p = (I + W_0\Delta)G$, where W_0 is the weight function, G_p is the uncertain model, and G is the nominal model. The input and output vector of Δ is marked as y_Δ and u_Δ, respectively. The input of the H∞ controller is $\vec{v} = \begin{bmatrix} i^*_{drf} - i_{drf}, & i^*_{qrf} - i_{qrf} \end{bmatrix}$. $\vec{w} = \begin{bmatrix} r, & d \end{bmatrix}$ and $\vec{z} = \begin{bmatrix} z_1, & z_2 \end{bmatrix}$ present the external disturbance vector and the weighted outputs, respectively.

$$\mathbf{A} = \frac{1}{L_s L_r - L_m^2} \begin{bmatrix} -L_r R_s & L_r L_s \omega_{sf} - L_m^2 \omega_{slip} & L_m R_r & L_m L_r \omega_{rf} \\ L_m^2 \omega_{slip} - L_r L_s \omega_{sf} & -L_r R_s & -L_m L_r \omega_{rf} & L_m R_r \\ L_m R_s & -L_m L_s \omega_{rf} & -L_s R_r & L_r L_s \omega_{slip} - L_m^2 \omega_{sf} \\ L_m L_s \omega_{rf} & L_m R_s & L_m^2 \omega_{sf} - L_r L_s \omega_{slip} & -L_s R_r \end{bmatrix}, \tag{11}$$

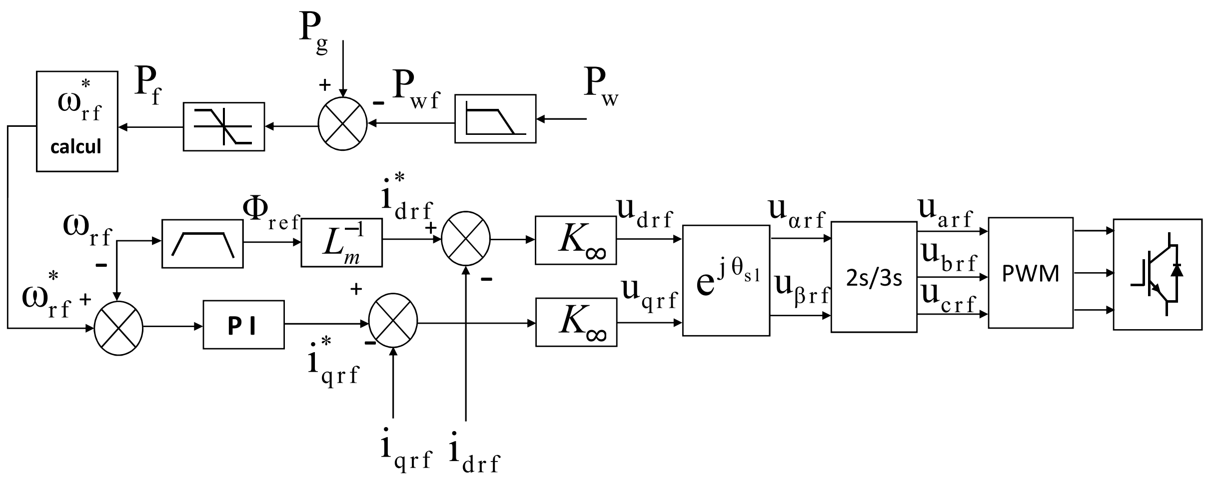

Fig. 3: Control Structure of the rotor side converter with H_∞ controllers.

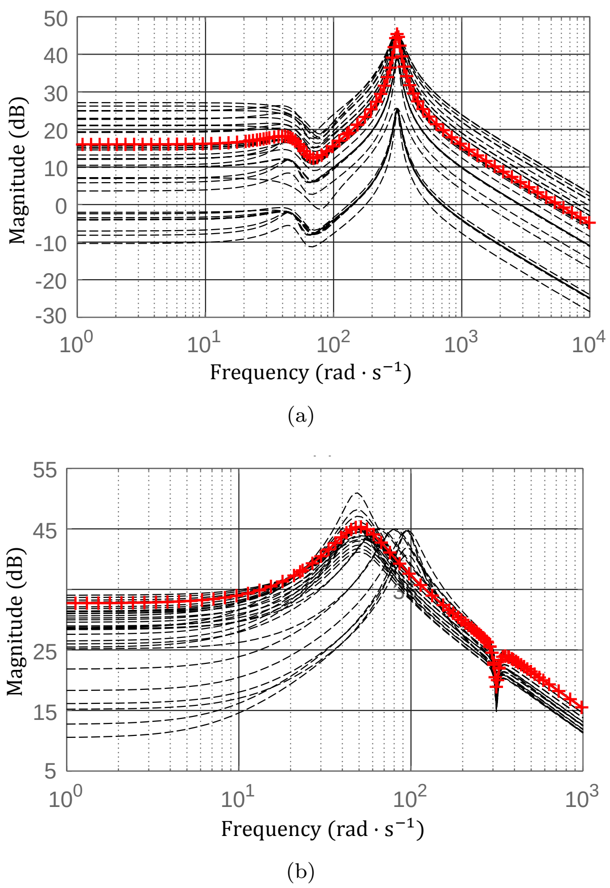

Fig. 4: Bode plots of the uncertain model (a) from u_{dsf} to i_{drf}, (b) from u_{drf} to i_{drf}.

$$\mathbf{B} = \frac{1}{L_m^2 - L_s L_r}\begin{bmatrix} -L_m & 0 \\ 0 & L_m \\ -L_s & -0 \\ 0 & -L_s \end{bmatrix}, \tag{12}$$

$$\mathbf{B_d} = \frac{1}{L_m^2 - L_s L_r}\begin{bmatrix} -L_r & 0 \\ 0 & -L_r \\ L_m & -0 \\ 0 & L_m \end{bmatrix}, \tag{13}$$

$$\mathbf{C} = \begin{bmatrix} 0 & 0 & 1 & 0 \\ 0 & 0 & 0 & 1 \end{bmatrix}. \tag{14}$$

The weighting functions W_1 and W_2 are used to shape v and u, respectively.

The block including G, G_d, W_0, W_1, and W_2 represents the shaped generalized plant P which can be derived as [23]:

$$\begin{bmatrix} y_\Delta \\ z \\ v \end{bmatrix} = \begin{bmatrix} P_{11}(s) & P_{12}(s) \\ P_{21}(s) & P_{22}(s) \end{bmatrix}\begin{bmatrix} u_\Delta \\ w \\ u \end{bmatrix} = \\ = \begin{bmatrix} 0 & 0 & G_d W_0 & G W_0 \\ 0 & 0 & 0 & W_2 \\ -W_1 & W_1 & -W_1 G_d & -W_1 G \\ -I & I & -G_d & -G \end{bmatrix}\begin{bmatrix} u_\Delta \\ w \\ u \end{bmatrix}. \tag{15}$$

The block including P and K represents the closed-loop system N which can be derived as:

$$N = F_l(P,K) = P_{11} + P_{12}K(I - P_{22}K)^{-1}P_{21} = \begin{bmatrix} -GW_0KS & GW_0KS & G_dW_0 - GW_0KSG_d \\ -W_2KS & W_2KS & -W_2KSG_d \\ W_1(GKS - I) & W_1(I - GKS) & W_1(GKS - I)G_d \end{bmatrix}, \tag{16}$$

where, $F_l(P, K)$ is the lower linear fractional transformation, and $S = (I + GK)^{-1}$ is the system sensitivity.

The design goal is to find a stabilizing controller K to minimize the H∞ norm of the closed-loop system N, which is the transfer function from external disturbances w to weighted outputs z:

$$\| N \|_\infty = \gamma_{\min} < \gamma, \tag{17}$$

where $\gamma_{\min}$ is obtained by solving two algebraic Riccati equations, and by reducing γ iteratively [28].

4.2. Weighting Functions Selection

The parameters uncertainties are represented in the frequency domain using multiplicative output uncertainty, and the relative errors of perturbed plants G_p can be expressed as [28]:

$$l_0(w) = \max_{w} \left| \frac{G_p(jw) - G(jw)}{G(jw)} \right|. \tag{18}$$

The design goal is to select a weight W_0 to cover the maximum magnitude of all relative error curves:

$$| W_0(jw) | \geq l_0(w), \ \forall w. \tag{19}$$

This can be achieved by using the following first-order filter:

$$W_0 = \frac{\tau s + r_0}{(\tau \cdot r_\infty^{-1})s + 1}, \tag{20}$$

Where τ^{-1} is approximately the frequency whereat the relative uncertainty reaches 100 %, r_0 is the relative uncertainty at steady state, and r_∞ is the magnitude of the weighting function at high frequency (typically, $r_\infty \geq 2$).

The corresponding relative errors and the weighting function W_0 are shown as functions of frequency in Fig. 6. It can be seen that the curve of W_0 lies at each frequency above all relative error curves.

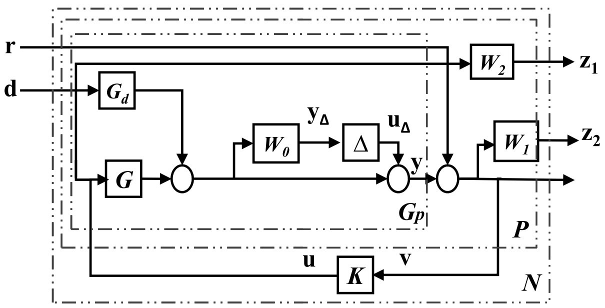

Fig. 5: The H∞ controller design.

W_1 must be designed to guarantee the tracking performance to the low-frequency reference signal and avoid high-frequency noises:

$$W_1 = \frac{\frac{s}{M_1} + w_1}{s + w_1 A_1}, \tag{21}$$

where $\frac{1}{|W_1|}$ is equal to $A_1 \leq 1$ at low frequencies, and equal to $M_1 \geq 1$ at high frequencies.

In order to avoid numerical problems in the algorithm used to synthesize the H_∞ controller, the weight W_1 was given a gain of 60 dB at low frequency instead of including a pure integrator.

On the other hand, W_2 is designed as a high-pass filter in order to limit the closed-loop bandwidth. The low frequency gain of W_2 was set as -100 dB to ensure that the function in Eq. (17) is dominated by W_1 at low frequencies.

$$W_2 = \frac{\frac{s}{M_2} + w_2}{s + w_2 A_2}. \tag{22}$$

The parameters of the weighting functions W_0, W_1, and W_2 are listed in Tab. 2.

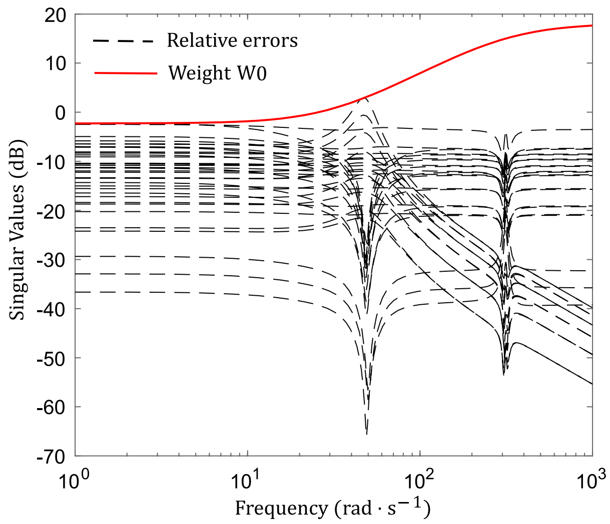

Fig. 6: The singular values curves of the weight W_0 and the relative errors.

4.3. Robust Stability and Robust Performance Analysis

The Robust Stability (RS) and Robust Performance (RP) of the proposed H_∞ controller should be validated to guarantee the system stability and control performance of all perturbed models.

The condition for robust stability of a system with a multiplicative output uncertainty can be expressed as follows [28]:

$$RS \Leftrightarrow \| T \|_{\infty} \left\| \frac{1}{W_0} \right\|_{\infty}, \ \forall \omega. \tag{23}$$

Figure 7 shows the singular value curves of the uncertain closed-loop system T and $1/W_0$. As can be seen, the maximum magnitude of all possible curves of T is below $1/W_0$ for all frequencies satisfying the RS condition in Eq. (23).

Tab. 2: Parameters of the weights.

Weights	Parameter	Value
W_0	r_0	0.77
	τ	0.025
	r_{∞}	8
W_1	M_1	15
	w_1	60
	A_1	0.001
W_2	M_2	15
	w_2	0.006
	A_2	10^6

The requirement of Robust Performance (RP) in the case of a system with multiplicative uncertainty is given in Eq. (24) [28]:

$$RS \Leftrightarrow \| W_1 S \|_{\infty} + \| W_0 T \|_{\infty} < 1, \ \forall \omega. \tag{24}$$

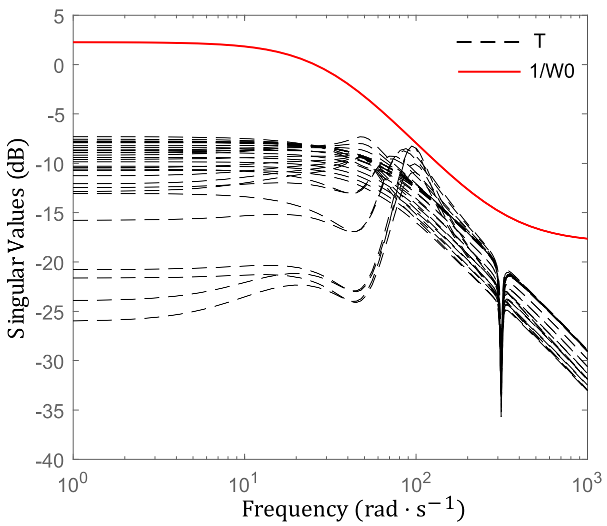

Fig. 7: Robust stability analysis.

Figure 8 illustrates the singular value curves of $\| W_1 S \|_{\infty} + \| W_0 T \|_{\infty}$ by considering all perturbed models. As can be seen, the maximum magnitude of all possible curves of $\| W_1 S \|_{\infty} + \| W_0 T \|_{\infty}$ is below 1 (0 dB) satisfying the RP condition in Eq. (24).

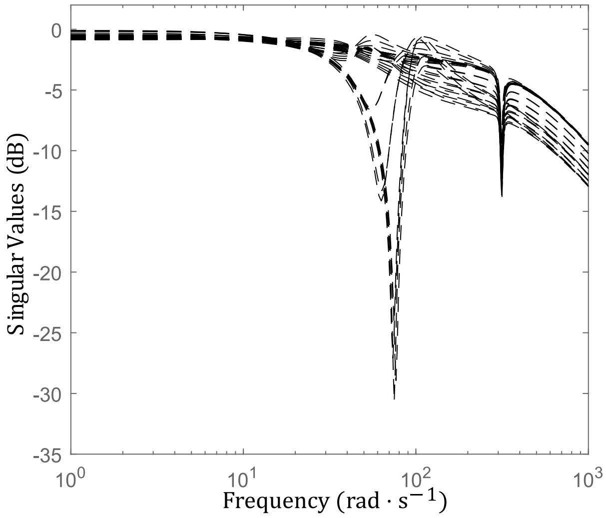

Fig. 8: The singular values curves for RP.

5. Simulation Tests

In order to examine the performance of the proposed H_{∞} current controller in the presence of voltage dips and WRIM parameter perturbation, the simulation model of 9 MW wind farm with 2 MW WRIM driven FESS has been constructed and simulated in Matlab/Simulink using SimPowerSystems. The parameters of the studied system are listed in App. A.

The FESS based WRIM is controlled to smooth the wind farm power output. The simulation results presented below were obtained for a desired active power at the grid of $P_g = -8$ MW.

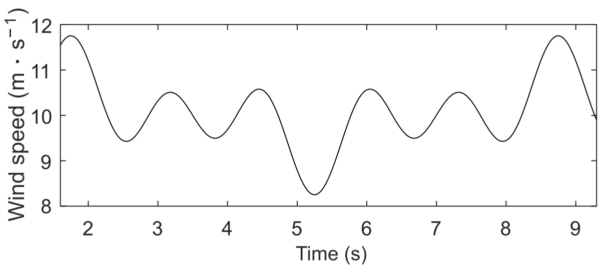

Fig. 9: Wind speed.

In first, a three-phase voltage dip of 20 % occurred from 5 s to 6 s. It is assumed that the wind speed variation is between 8 m·s^{-1} and 12 m·s^{-1} as shown in Fig. 9. Therefore, the wind farm generates the maximum active power from the wind, as shown in Fig. 10. The rotor speed variation of the FESS is shown in Fig. 11.

When active power is required by the grid, the rotor speed is decreasing and the WRIM runs as a generator extracting power from the flywheel storage system and injecting it into the grid. When wind energy is required to be stored in the flywheel, the WRIM runs as a motor and the rotor speed is increasing to charge the flywheel storage system.

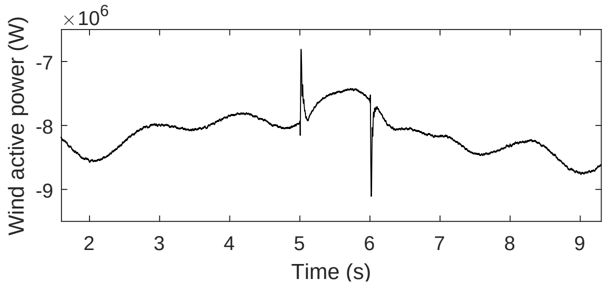

Fig. 10: Wind farm active power with voltage dip.

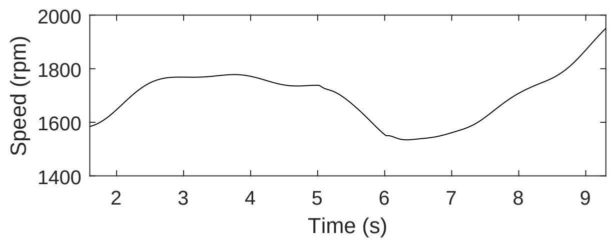

Fig. 11: WRIM rotor speed with voltage dip.

Here, the PI controller of the rotor current loop was also simulated to compare the performance with the proposed H_∞ current controller. The behavior of the WRIM rotor currents as controlled by the PI and H_∞ controllers in the presence of voltage dip are shown in Fig. 12 and Fig. 13, respectively.

Figure 12 displays the WRIM rotor currents (Fig. 12(a)) and their zoom (Fig. 12(b)) in the case of the PI current controller. It is very clear to seed that the voltage dip causes the WRIM rotor currents to distort. While the same voltage dip has no impact on WRIM rotor currents in the case of the proposed H_∞ current controller, as shown in Fig. 13. The comparisons show that the over-currents in the rotor windings of the WRIM can be well limited with the proposed H_∞ controller, which can enhance the capability of the WRIM driven FESS to withstand voltage dips.

Figure 14 presents the WRIM active power (Fig. 14(a)) and its zoom (Fig. 14(b)) controlled by PI and H_∞ controllers in the presence of voltage dip. We can observe that the active power presents oscillations under voltage dip in the case of PI controller. While the H_∞ controller reduces the oscillations produced by the voltage dip on the WRIM active power. The above-described simulations demonstrate the capability of the FESS to inject more clean power to the grid.

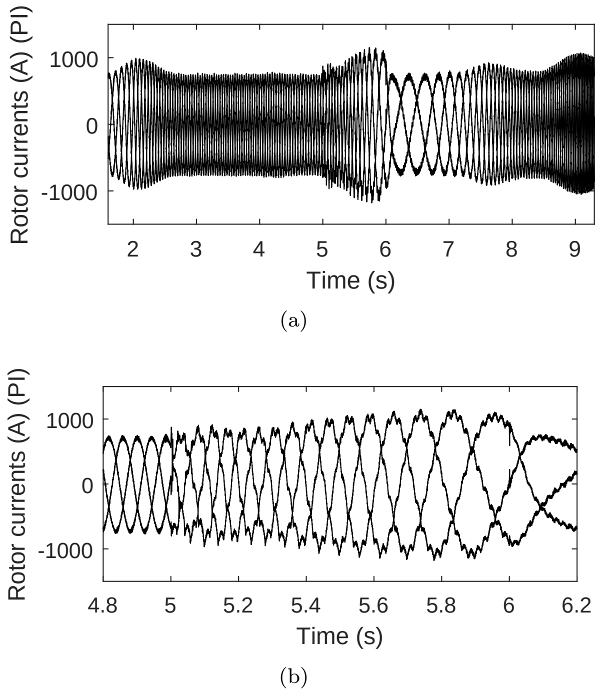

Fig. 12: Influence of dip voltage on PI controller (a) WRIM rotor currents (b) Zoom of the rotor currents.

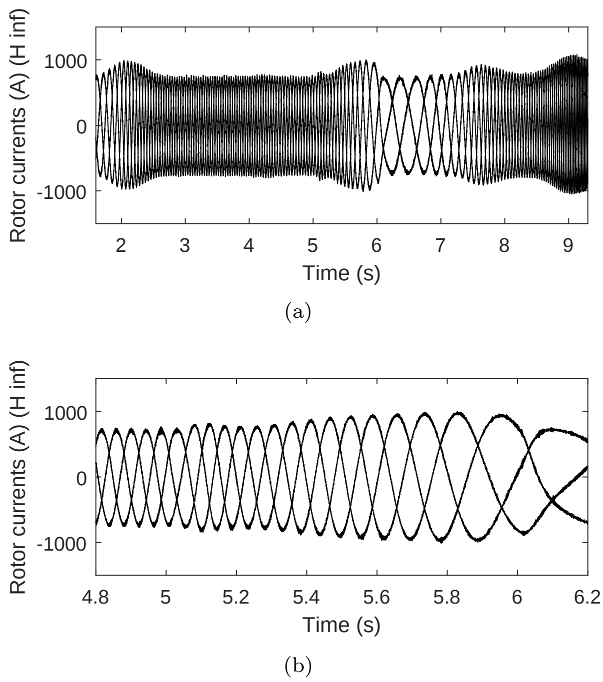

Fig. 13: Influence of voltage dip on H_∞ controller (a) WRIM rotor currents (b) Zoom of the WRIM rotor currents.

Figure 15 shows the grid active power (Fig. 15(a)) and its zoom (Fig. 15(b)) in the case of the PI and

H_∞ current controllers. As can be seen, the voltage dip produces oscillations on the active power injected into the grid in the case of PI controller. While, the voltage dip has less impact on the active power injected into the grid in the case of the proposed H_∞ current controller, which helps to ameliorate the quality of the grid active power in the presence of voltage dip.

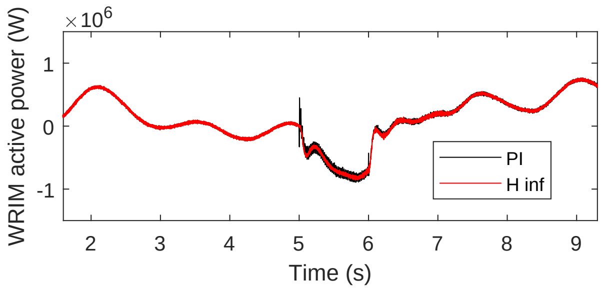

(a)

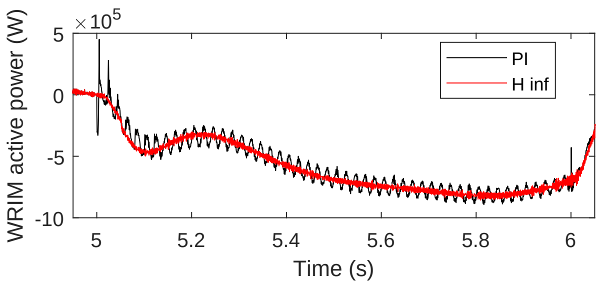

(b)

Fig. 14: Influence of voltage dip on PI and H_∞ controllers (a) WRIM active power (b) Zoom of the WRIM active power.

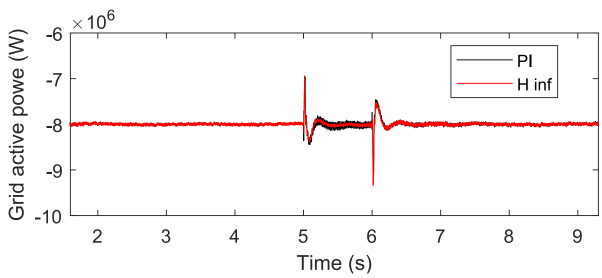

(a)

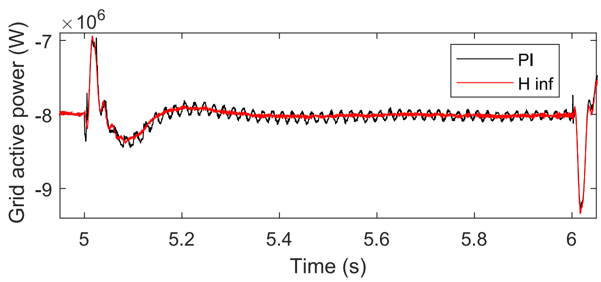

(b)

Fig. 15: Influence of voltage dip on PI and H_∞ controllers (a) Grid active power (b) Zoom of the grid active power.

Furthermore, parameter variations often occur in real-time control, which can degrade the WRIM driven FESS performance. In the aim to test the impact of the WRIM parameter perturbation on the system performance, simulations were made supposing that the values of L_m, L_s, L_r and R_r are increased by 30 %.

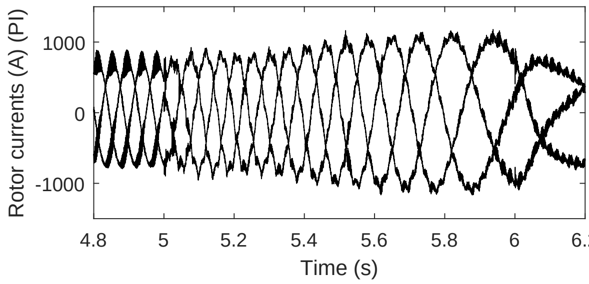

(a)

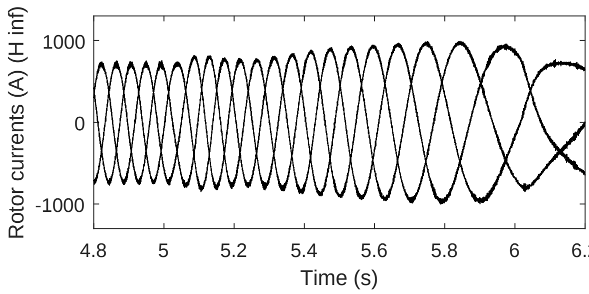

(b)

Fig. 16: Zoom of WRIM rotor currents under voltage dip with parameter perturbation.

Figure 16 and Fig. 17 show the comparison between the PI controller and the proposed H_∞ controller under parameter perturbation and for the same voltage dip. In Fig. 16, we can observe that the WRIM parameter perturbation has less effect on the rotor currents using the proposed H_∞ controller. While in the case of PI controller, the rotor currents present severe distortion which may threaten the safe operation of the FESS.

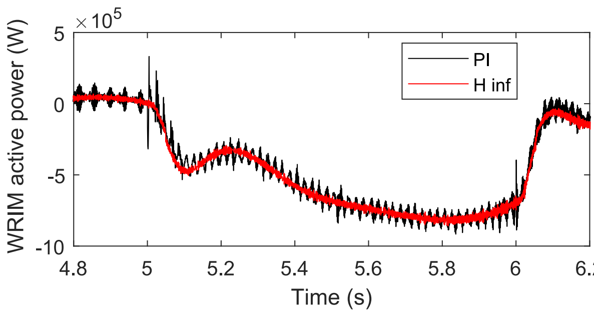

Fig. 17: Zoom of WRIM active power under voltage dip with parameter perturbation.

Figure 17 displays the WRIM active power zoom under voltage dip with parameter perturbation. It is shown that the WRIM parameter perturbation has an important effect on the active power controlled by the conventional PI controller, while this impact is effectively reduced by the H_∞ controller.

The comparisons show that the proposed H_∞ controller has excellent performance under voltage dip and is robust to WRIM parameter perturbation.

6. Conclusion

This work proposes a robust H_∞ control scheme for a Wound Rotor Induction Machine (WRIM) driven Flywheel Energy Storage System (FESS) connected to the grid. The proposed H_∞ controller is used to limit the rotor over-current, and enhance its Robust Stability (RS) and Robust Performance (RP) under grid voltage dips with parameter perturbation. The H_∞ controller is designed using a modified mixed-sensitivity synthesis based multiplicative output uncertainty. Weighting functions are selected in this design to decrease the negative effects of grid voltage dips and to guarantee the RS and RP of the proposed H_∞ controller under parameter perturbation.

The comparison between PI and H_∞ controller for the WRIM rotor currents and active power control is investigated, taking into consideration robustness to grid voltage dips and WRIM parameter perturbation. The simulation results illustrate that the proposed H_∞ controller has excellent performance compared with the PI one. Moreover, the proposed H_∞ control scheme leads to smooth the wind farm power output and ensures better quality of wind power generation under grid voltage dips.

Experiments will be conducted in the future work to validate the proposed control strategy.

References

[1] Global Wind Report. In: *Global Wind Energy Council* [online]. 2018. Available at: `https://gwec.net/global-wind-report-2018/`.

[2] SERBAN, E., M. ORDONEZ and C. PONDICHE. Voltage and Frequency Grid Support Strategies Beyond Standards. *IEEE Transactions on Power Electronics*. 2017, vol. 32, iss. 1, pp. 298–309. ISSN 1941-0107. DOI: 10.1109/TPEL.2016.2539343.

[3] VAN, T. L., T. D. NGYEN, T. T. TRAN and H. D. NGUYEN. Advanced Control Strategy of Back-to-Back PWM Converters in PMSG Wind Power System. *Advances in Electrical and Electronic Engineering*. 2015, vol. 13, iss. 2, pp. 81–95. ISSN 1804-3119. DOI: 10.15598/aeee.v13i2.1161.

[4] YAO, J., M. YU, W. GAO and X. ZENG. Frequency regulation control strategy for PMSG wind-power generation system with flywheel energy storage unit. *IET Renewable Power Generation*. 2017, vol. 11, iss. 8, pp. 1082–1093. ISSN 1752-1424. DOI: 10.1049/iet-rpg.2016.0047.

[5] GAYATHRI, N. S., N. SENROY and I. N. KAR. Smoothing of wind power using flywheel energy storage system. *IET Renewable Power Generation*. 2017, vol. 11, iss. 3, pp. 289–298. ISSN 1752-1424. DOI: 10.1049/iet-rpg.2016.0076.

[6] MIR, A. S. and N. SENROY. Intelligently Controlled Flywheel Storage for Enhanced Dynamic Performance. *IEEE Transactions on Sustainable Energy*. 2019, vol. 10, iss. 4, pp. 2163–2173. ISSN 1949-3037. DOI: 10.1109/TSTE.2018.2881317.

[7] ABDELTAWAB, H. H. and Y. A. I. MOHAMED. Robust Energy Management of a Hybrid Wind and Flywheel Energy Storage System Considering Flywheel Power Losses Minimization and Grid-Code Constraints. *IEEE Transactions on Industrial Electronics*. 2016, vol. 63, iss. 7, pp. 4242–4254. ISSN 1557-9948. DOI: 10.1109/TIE.2016.2532280.

[8] ZHANG, X. and J. YANG. A DC-Link Voltage Fast Control Strategy for High-Speed PMSM/G in Flywheel Energy Storage System. *IEEE Transactions on Industry Applications*. 2018, vol. 54, iss. 2, pp. 1671–1679. ISSN 1939-9367. DOI: 10.1109/TIA.2017.2783330.

[9] CIMUCA, G., S. BREBAN, M. M. RADULESCU, C. SAUDEMONT and B. ROBYNS. Design and Control Strategies of an Induction-Machine-Based Flywheel Energy Storage System Associated to a Variable-Speed Wind Generator. *IEEE Transactions on Energy Conversion*. 2010, vol. 25, iss. 2, pp. 526–534. ISSN 1558-0059. DOI: 10.1109/TEC.2010.2045925.

[10] GHOSH, S. and S. KAMALASADAN. An Integrated Dynamic Modeling and Adaptive Controller Approach for Flywheel Augmented DFIG Based Wind System. *IEEE Transactions on Power Systems*. 2017, vol. 32, iss. 3, pp. 2161–2171. ISSN 1558-0679. DOI: 10.1109/TPWRS.2016.2598566.

[11] ABDEL-KHALIK, A. S., A. A. ELSEROUGI, A. M. MASSOUD and S. AHMED. Fault Current Contribution of Medium Voltage Inverter and Doubly-Fed Induction-Machine-Based Flywheel Energy Storage System. *IEEE Transactions on Sustainable Energy*. 2013,

vol. 4, iss. 1, pp. 58–67. ISSN 1949-3037. DOI: 10.1109/TSTE.2012.2198926.

[12] ZIAEI, A., R. GHAZI and R. Z. DAVARANI. Linear Modal Analysis of Doubly-Fed Induction Generator (DFIG) Torsional Interaction: Effect of DFIG Controllers and System Parameters. *Advances in Electrical and Electronic Engineering*. 2018, vol. 16, iss. 4, pp. 388–401. ISSN 1804-3119. DOI: 10.15598/aeee.v16i4.2265.

[13] KAIROUS, D. and R. WAMKEUE. DFIG-based fuzzy sliding-mode control of WECS with a flywheel energy storage. *Electric Power Systems Research*. 2012, vol. 93, iss. 1, pp. 16–23. ISSN 0378-7796. DOI: 10.1016/j.epsr.2012.07.002.

[14] ABDEL-KHALIK, A., A. ELSEROUGI, A. MASSOUD and S. AHMED. A power control strategy for flywheel doubly-fed induction machine storage system using artificial neural network. *Electric Power Systems Research*. 2013, vol. 96, iss. 1, pp. 267–276. ISSN 0378-7796. DOI: 10.1016/j.epsr.2012.11.012.

[15] ALOLAH, A. I., H. M. HASANIEN, S. M. MUYEEN and T. A. TAJ. Transient stability enhancement of a grid-connected wind farm using an adaptive neuro-fuzzy controlled-flywheel energy storage system. *IET Renewable Power Generation*. 2015, vol. 9, iss. 7, pp. 792–800. ISSN 1752-1424. DOI: 10.1049/iet-rpg.2014.0345.

[16] RAN, L., D. XIANG and J. L. KIRTLEY. Analysis of Electromechanical Interactions in a Flywheel System With a Doubly Fed Induction Machine. *IEEE Transactions on Industry Applications*. 2011, vol. 47, iss. 3, pp. 1498–1506. ISSN 1939-9367. DOI: 10.1109/TIA.2011.2127436.

[17] LAZRAK, A. and A. ABBOU. H_∞ current controller of WRIM based flywheel storage system under unbalanced stator voltage. *International Journal of Renewable Energy Research*. 2019, vol. 9, no. 2, pp. 613–623. ISSN 1309-0127.

[18] SHIHABUDHEEN, K. V., G. N. PILLAI and S. K. RAJU. Neuro-Fuzzy Control of DFIG Wind Energy System with Distribution Network. *Electric Power Components and Systems*. 2019, vol. 46, iss. 13, pp. 1416–1431. ISSN 1532-5008. DOI: 10.1080/15325008.2018.1499154.

[19] DJILALI, L., E. N. SANCHEZ and M. BELKHEIRI. Real-time neural sliding mode field oriented control for a DFIG-based wind turbine under balanced and unbalanced grid conditions. *IET Renewable Power Generation*. 2019, vol. 13, iss. 4, pp. 618–632. ISSN 1752-1424. DOI: 10.1049/iet-rpg.2018.5002.

[20] LAZRAK, A. and A. ABBOU. An Improved Control Strategy for DFIG Wind Turbine to Ride-Through Voltage Dips. In: *6th International Renewable and Sustainable Energy Conference*. Rabat: IEEE, 2018, pp. 1–6. ISBN 978-1-7281-1182-7. DOI: 10.1109/IRSEC.2018.8703017.

[21] SUN, D., X. WANG, H. NIAN and Z. Q. ZHU. A Sliding-Mode Direct Power Control Strategy for DFIG Under Both Balanced and Unbalanced Grid Conditions Using Extended Active Power. *IEEE Transactions on Power Electronics*. 2018, vol. 33, iss. 2, pp. 1313–1322. ISSN 1941-0107. DOI: 10.1109/TPEL.2017.2686980.

[22] JERIN, A. R. A., P. KALIANNAN, U. SUBRAMANIAM and M. S. EL MOURSI. Review on FRT solutions for improving transient stability in DFIG-WTs. *IET Renewable Power Generation*. 2018, vol. 12, iss. 15, pp. 1786–1799. ISSN 1752-1424. DOI: 10.1049/iet-rpg.2018.5249.

[23] WANG, Y., Q. WU, R. YANG, G. TAO and Z. LIU. H_∞ current damping control of DFIG based wind farm for sub-synchronous control interaction mitigation. *International Journal of Electrical Power & Energy Systems*. 2018, vol. 98, iss. 1, pp. 509–519. ISSN 0142-0615. DOI: 10.1016/j.ijepes.2017.12.003.

[24] WILLMANN, G., D. F. COUTINHO, L. F. A. PEREIRA and F. B. LIBANO. Multiple-Loop H-Infinity Control Design for Uninterruptible Power Supplies. *IEEE Transactions on Industrial Electronics*. 2007, vol. 54, iss. 3, pp. 1591–1602. ISSN 1557-9948. DOI: 10.1109/TIE.2007.894721.

[25] LI, Y. W., D. M. VILATHGAMUWA, F. BLAABJERG and P. C. LOH. A Robust Control Scheme for Medium-Voltage-Level DVR Implementation. *IEEE Transactions on Industrial Electronics*. 2007, vol. 54, iss. 4, pp. 2249–2261. ISSN 1557-9948. DOI: 10.1109/TIE.2007.894771.

[26] ZHU, C., M. KHAMMASH, V. VITTAL and W. QIU. Robust power system stabilizer design using H_∞ loop shaping approach. *IEEE Transactions on Power Systems*. 2003, vol. 18, iss. 2, pp. 810–818. ISSN 1558-0679. DOI: 10.1109/TPWRS.2003.811176.

[27] LAZRAK, A. and A. ABBOU. Robust Power Control of DFIG Based Wind Turbine without Currents Rotor Sensor. In: *International Renewable and Sustainable Energy Conference (IRSEC)*. Tangier: IEEE, 2017, pp. 1–6. ISBN 978-1-5386-2847-8. DOI: 10.1109/IRSEC.2017.8477340.

[28] SKOGESTAD, S. and I. POSTLETHWAITE. *Multivariable Feedback Control: Analysis and Design*. 2nd ed. New York: Wiley, 2005. ISBN 978-0-470-01167-6.

[29] LAZRAK, A., A. ABBOU and M. SIDKI. Power control of DFIG based wind turbine during stator voltage drop. In: *3rd International Renewable and Sustainable Energy Conference*. Marrakech: IEEE, 2015, pp. 1–7. ISBN 978-1-4673-7894-9. DOI: 10.1109/IRSEC.2015.7455100.

[30] MERAL, M. E. and D. CELIK. DSOGI-PLL Based Power Control Method to Mitigate Control Errors Under Disturbances of Grid Connected Hybrid Renewable Power Systems. *Advances in Electrical and Electronic Engineering*. 2018, vol. 16, iss. 1, pp. 81–91. ISSN 1804-3119. DOI: 10.15598/aeee.v16i1.2485.

[31] NOVOTNY, D. W. and T. A. LIPO. *Vector Control and Dynamics of AC Drives*. 1st ed. Oxford: Oxford University Press, 1996. ISBN 978-0-198-56439-3.

About Authors

Ahmed LAZRAK was born in Agadir, Morocco. He received his B.Sc. degree in Electromechanical and Automated Systems from Higher Normal School of Technical Education, Mohammed V University Rabat, Morocco in 2010, and M.Sc. degree in Electronic Systems of Aviation Safety from Mohammed VI International Academy of Civil Aviation, Morocco. He is currently in the process of preparing the Ph.D. degree in electrical engineering in Mohammadia School of Engineering, Mohammed V University Rabat, Morocco, and his research interests include robust control of electric drives, wind power generation, flywheel storage systems and power quality.

Ahmed ABBOU was born in Agadir, Morocco. He received the Ph.D. degree from Mohammadia School of Engineering, Mohammed V University Rabat, Morocco in 2009, and the M.Sc. from Mohammadia School of Engineer in 2005. Since 2009, he has been working at Mohammadia School of Engineering in Rabat, where he is a professor of Power Electronics and Electric drives. He published numerous papers in international journals and conferences. His research interests include electric drives and control, senseless drives for AC machines, renewable energy (PV and wind energy).

Appendix A

WRIM FESS Parameters

- Grid frequency: $f = 50$ Hz,
- Stator voltage: $V_S = 690$ V,
- Rated power: $P_N = 2$ MW,
- Rated rotational speed: $n = 1500$ rpm,
- Pair poles: $p = 2$,
- Stator resistance: $R_S = 0.0026\ \Omega$,
- Rotor resistance: $R_r = 0.0029\ \Omega$,
- Stator inductance: $L_S = 0.0026$ H,
- Rotor inductance: $L_r = 0.0026$ H,
- Magnetizing inductance: $L_m = 0.0025$ H,
- DC bus voltage: $V_{bus} = 1150$ V,
- Inertia: $J = 127$ kg·m^2,
- DC bus capacitor: $C = 80 \cdot 10^{-3}$ F.

Wind Turbine Parameters

- Rated wind speed: $v_w = 12$ m·s^{-1},
- Rated power: $P_n = 1.5$ MW,
- Radius: $R = 35.25$ m,
- Total inertia: $J_T = 1000$ kg·m^2,
- Gear box: $G = 90$,
- Air density: $\sigma = 1.225$ kg·m^{-3},
- $R_S = 0.012\ \Omega$,
- $R_r = 0.021\ \Omega$,
- $L_S = 0.0137$ H,
- $L_r = 0.0136$ H,
- $L_m = 0.0135$ H.